Title page

Turbulent Flows over Real Heterogeneous Urban Surfaces: Wind Tunnel Experiments and Reynolds-Averaged Navier-Stokes Simulations

Wai-Chi Cheng[a,b], Chun-Ho Liu[*,c], Yat-Kiu Ho[c], Ziwei Mo[c], Zhangquan Wu[c], Wenye Li[c], Lilian Y.L. Chan[d], W.K. Kwan[d], Hing Tuen Yau[d]

[a]School of Atmospheric Sciences, and Guangdong Province Key Laboratory for Climate Change and Natural Disaster Studies, Sun Yat-sen University, Zhuhai, China
[b]Southern Marine Science and Engineering Guangdong Laboratory (Zhuhai), Zhuhai, China
[c]Department of Mechanical Engineering, The University of Hong Kong, Hong Kong
[d]Information Technology Services, The University of Hong Kong, Hong Kong

*Corresponding Author: Department of Mechanical Engineering, 7/F Haking Wong Building, The University of Hong Kong, Pokfulam Road, Hong Kong; Tel: +852 3917 7901 / +852 9788 7951; Fax: +852 2858 5415; Email address: liuchunho@graduate.hku.hk; URL: https://aplhk.tech

Acknowledgements

This research is conducted in part using the research computing facilities and/or advisory services offered by Information Technology Services (ITS), The University of Hong Kong (HKU). Yat-Kiu Ho and Zhangquan Wu thank the Hong Kong (HK) Research Grants Council (RGC) for the financial support through the Hong Kong Ph.D. Fellowship (HKPF) Scheme. This study is partly supported by the RGC Theme-based Research Scheme (TRS) T24-504/17-N, the RGC Collaborative Research Fund (CRF) C7064 18G as well as the National Natural Science Foundation of China and Macau Science and Technology Development Joint Fund (NSFC-FDCT), China and Macau (41861164027).

Abstract

Wind tunnel experiment and steady-state Reynolds-averaged Navier-Stokes (RANS) approaches are used to examine the urban boundary layer (UBL) development above Kowloon Peninsula, Hong Kong Special Administrative Region (HKSAR). The detailed urban morphology is resolved by computational fluid dynamics (CFD) and is fabricated by 3D-printing (reduced scale) for wind tunnel experiments. Different from the majority existing results based on idealized, homogeneous urban geometries, it was found that the wind and turbulence in the UBL over downtown Kowloon are characterized by the wake behind several high-rise buildings. In particular, local maxima of turbulence kinetic energy (TKE) and shear stress are found at the roof level of those high-rise buildings. In the downstream region where the flows are already adjusted to the urban surfaces, the urban roughness sublayer (URSL) can be further divided into two layers based on the structures of the mixing length l_m, effective drag D_x and dispersive stress. In the lower URSL ($z \leq 100$ m), l_m is rather uniform, and the Reynolds stress and dispersive stress are comparable. In the upper URSL (100 m $\leq z \leq 300$ m), on the contrary, l_m is peaked at the mid-height and the magnitude of dispersive stress is smaller than that of the Reynolds stress (< 30%). The effective drag D_x is negligible in the upper URSL.

Keywords: Computational Fluid dynamics (CFD), Real urban morphology, Urban boundary layer (UBL), Urban canopy model (UCM), Wind tunnel experiments

Main text

1. Introduction

Air quality and thermal comfort, which are closely related to city planning and development, are crucial to the health of urban inhabitants. Laboratory experiments and mathematical models have been adopted to study the flows over two-dimensional (2D) street canyons (Barlow and Belcher 2002; Letzel et al. 2008; Cheng and Liu 2011; Castro 2012; Mo and Liu 2018; Wu and Liu 2018) and three-dimensional (3D) building arrays (Raupach 1992; Coceal and Belcher 2004; Castro et al. 2006; Cheng and Porté-Agel 2015, 2016). The results have paved the fundamentals of winds and turbulence above homogeneous, idealized urban surfaces. Sensitivity of urban flows to various key geometric factors, such as aspect ratios and frontal/plan area indices, have been tested that facilitated the parameterization of roughness length z_0 and zero-plane displacement height d (Raupach, 1992; Grimmond and Oke, 1999; Yang and Meneveau, 2016). In the air quality perspective, the dispersion coefficient for idealized urban surfaces has been proposed as well (Hamlyn et al., 2007; Belcher et al., 2015; Goulart et al., 2018; Mo and Liu, 2018). These studies have provided valuable information for the thorough understanding of the physical processes in urban boundary layers (UBLs).

The aforementioned results are also useful to the parametrization of flows over idealized urban canopies (Raupach and Shaw, 1982; Finnigan, 2000; Coceal and Belcher, 2005). Using wind tunnel experiments, Macdonald (2000) proposed an urban canopy model (UCM) by assuming uniform mixing length l_m below the building roof level. Afterward, Coceal and Belcher (2004) improved the formulation of length scale by interpolating inside and over the urban canopies. Although its validity is questionable, assuming uniform l_m would simplify the mean wind speeds to exponential profiles (Castro, 2017). In more recent studies, explicit calculations of the vertical l_m profile have been carried out by direct numerical simulation (DNS; Coceal et al. 2006) and large-eddy simulation (LES; Kono et al. 2010; Cheng and Porté-Agel 2015; Castro 2017). Consistently, a local maximum was found at about the mid-height of the canopies. The drag coefficient for blocks with different densities has been determined experimentally (Cheng and Castro, 2002; Castro, 2017) as well as numerically (Santiago et al., 2008; Leonardi and Castro, 2010). Hang and Li (2010, 2012) used another approach by treating urban surface as a porous media and developed macroscopical models to parametrize the effects of urban surface on the ABL. Whereas, an UCM, which is applicable to a wide range of urban canopies, is not yet available.

Real urban surfaces are highly heterogeneous in terms of architectural parameters such as the packing density, height and orientation of buildings (e.g. Asian and

European cities). Currently, the effect of urban heterogeneity on UBL flows remains poorly understood (Barlow et al., 2017). Over the years, studies have been carried out to characterize the turbulence in the roughness sublayers (RSLs) above heterogeneous urban surfaces using laboratory experiments (Hanna et al., 2006; Hertwig et al., 2012), computational fluid dynamics (CFD; Xie and Castro 2009; Gousseau et al. 2011; Blocken et al. 2012; Antoniou et al. 2017) and morphological models (Ng et al., 2011). It is challenging to resolve the broad spectra of turbulence scales close to highly heterogeneous urban surfaces experimentally or numerically. Most of the existing results were case studies of ventilation behavior and pollutant dispersion that adopted semi-idealized urban configurations (Xie and Castro, 2009; Antoniou et al., 2017; Ricci et al., 2017; Efthimiou et al., 2015; Toparlar et al., 2015; Hertwig et al., 2012; Tominaga et al., 2015; Gao et al., 2018; Tolias et al., 2018) or only considered part of a neighborhood (1 km) with simple building geometry (Gousseau et al., 2011, 2015; Neophytou et al., 2011; Ng et al., 2011; Nozu and Tamura, 2012; Yuan et al., 2014; Giometto et al., 2016; Wang and Ng, 2018). More quantitative studies of city-scale flows and pollutant dispersion (10 km) with buildings properly resolved are thus needed.

In view of the aforementioned knowledge gap, the objectives of this study are to:

1. develop novel experimental and CFD methods to simulate UBL flows; and

2. characterize the UBL development above real, heterogeneous urban surfaces.

In Section 2, the wind tunnel experiments and the RANS simulations are introduced. Section 3 compares the results as well as characterizes the UBL development. Finally, conclusions are drawn in Section 4.

2. Methodology

Part of Kowloon Peninsula, with an area of approximately 6 km × 0.5 km, is modeled to investigate the effect of real heterogeneous urban morphology on UBL flows (Fig. 1). It is one of the downtown areas in Hong Kong Special Administrative Region (HKSAR) where is covered by diversified buildings including the skyscrapers in Tsim Sha Tsui, the residential areas in Yau Ma Tei and the commercial zones in Mong Kok. There are over 3,000 buildings in the region with an average building height of 25 m. More than 98% of the buildings are shorter than 80 m (Fig. 2) and five are over 150 m (not shown in the figure). Southerly winds are adopted. As the building configuration is relatively uniform and the terrain is relatively flat (< 65 m above sea level), it provides an ideal condition to study the UBL development above real urban surfaces.

The urban morphology is collected from the Survey and Mapping Office of Lands Department, HKSAR (Hong Kong Lands Department, 2018). The 3D spatial data, which are formatted in virtual reality modeling language (VRML), describe the detailed

ground features (buildings, infrastructures and terrain). They are converted to stereolithography (STL) before model fabrication for the wind tunnel experiments and CFD mesh generation. The 3D-printing, physical model is 1:1,500 (reduced-scale; Fig. 3).

The building frontal area index

$$\lambda_f = \frac{A_f}{A_p} \quad (1)$$

is one of the parameters characterizing urban morphology. Here, A_f is the total facade area projected onto the plane normal to the prevalent flows and A_p the ground plane area (Grimmond and Oke, 1999). In northeasterly or southeasterly winds, λ_f of Kowloon Peninsula varies from 0.15 (city parks) to 0.9 (Mong Kok and Tsim Sha Tsui). In most of the region λ_f is higher than 0.3 except the city parks (Wong et al., 2010). In southerly winds, similar values of λ_f are expected.

2.2. Wind Tunnel Experiments

The laboratory experiments are carried out in the isothermal, open-circuit wind tunnel in the Department of Mechanical Engineering, The University of Hong Kong. The wind tunnel sizes 6 m (long) × 0.56 m (width) × 0.56 m (height). In order to replicate the ABL approaching winds in the wind tunnel, LEGO^{TM} roughness elements are mounted upstream of the test section for the development of turbulent boundary

layer (TBL) incoming flow. The Reynolds number Re ($= U_0 H_c/\nu$; where H_c is the height of tallest building (Building "C") in the domain, U_0 the free-stream wind speed and ν the kinematic viscosity of air) is about 10^5. The specification of the wind tunnel was detailed elsewhere (Leung et al., 2012; Leung and Liu, 2012).

The sampling probe is positioned by a computer-control traversing system and the National Instruments (NI) motion control unit. The velocities are sampled by our in-house made X-wire probe of constant-temperature (CT) hot-wire anemometer (HWA). The pair of 5-μm-diameter platinum-plated tungsten wires have effective length of 0.2 mm (partly etched) and an included angle of 90°. The analog CT HWA signal is digitalized by a 24-bit NI data acquisition module (NI 9239; offset error ±0.05% for analog input 10:52 V) mounted in a NI Compact DAQ chassis (NI cDAQ-9188). The NI units are connected to a digital computer via local area network (LAN) and the data sampling is managed by LabVIEW software. The sampling time at each point is 60 sec and the sampling frequency is 2 kHz that are comparable to those employed in literature (Cheng and Castro, 2002). The CT HWA has been calibrated according to the universal law of the Institute of Sound and Vibration (ISVR; Bruun 1971). Its readings are also compared with those monitored by a Pitot tube of which the uncertainty is less than 3% and the correlation coefficient is up to 0:9997.

Flows are sampled over the Mong Kok region on a vertical $(x - z)$ plane at $y = -0.1$ m ($y = 0$ is the domain mid-plane; Fig. 3). In particular, measurements along five vertical profiles are used to validate the RANS simulation in this paper. The vertical sampling resolution is 10^{-3} m near the building and 10^{-2} m in the free stream.

2.3. CFD RANS Simulation

RANS simulations of flows similar to those of the wind tunnel experiments are performed. The CFD results are used to investigate UBL development above real urban surface. The open-source CFD code, OpenFOAM (OpenFOAM, 2020), is used to perform the steady-state RANS simulations. Incompressible flows in isothermal conditions are considered. The renormalization group (RNG) $k - \varepsilon$ turbulence model (Ferziger and Peric, 2002; Yakhot and Orszag, 1992) is used because of its remarkable performance handling recirculating flows (Zhai et al., 2007).

The computational domain is discretized into finite volume (FV) cells by the OpenFOAM utilities *blockMesh* and *snappyHexMesh* (Fig. 4). Its sizes are L_x (= 4,050 m) × L_y (= 810 m) × L_z (= 1,200 m) in the streamwise x, spanwise y and vertical z directions, respectively. A higher L_z compared with that in the wind tunnel experiment is adopted in the RANS simulations to reduce the building blockage. The blockage ratios of the wind tunnel experiment and the RANS simulations are estimated to be 3%

and 2%, respectively. Moreover, the lateral boundaries are located in close proximity to the buildings. This facilitates the UBL development downstream of the coastline in Tsim Sha Tsui that is analogous to the 2D internal boundary layer (IBL) simulated in Cheng and Porté-Agel (2015, 2016).

Neutral TBL in flows are prescribed in the form of power-law wind profile

$$\bar{u} = U_s \left(\frac{z}{z_s}\right)^{\alpha} \quad \text{and} \quad \bar{v} = \bar{w} = 0 \tag{2}$$

at the domain inlet. Here, $\bar{u}$ is the mean streamwise velocity, $\bar{v}$ the spanwise, $\bar{w}$ the vertical, z the height, U_s the wind speed at the reference height z_s (=300 m) and α (= 0.2) the wind-profile exponent. Following the guidelines proposed by Tominage et al. (2008), the turbulence kinetic energy (TKE) k and TKE dissipation rate ε at the inlet are prescribed as

$$k = 0.0025 U_s^2 \left(\frac{z}{z_s}\right)^{-0.1} \tag{3}$$

and

$$\varepsilon = C_\mu^{1/2} k \frac{U_s}{z_s} \left(\frac{z}{z_s}\right)^{\alpha-0.1} \tag{4}$$

respectively, where C_μ (= 0.09) is a modeling constant. Using these profiles in turn assumes the local balance between the production and dissipation of TKE. Symmetry boundary conditions (BCs) are used at the domain top and the lateral boundaries. An outflow BC is used at the outlet. A wall model based on the logarithmic wind profile

(Spalding, 1961) with z_0 equals to 0.1 m is used on the facades and the ground surfaces. The Reynolds number Re (= $U_0 H_c/\nu$) is about 10^6.

The second-order accurate Gaussian integration and the linear upwind scheme are used to calculate the gradient and the divergence terms, respectively. The Semi-Implicit Method for Pressure Linked Equations (SIMPLE) is used to handle the velocity-pressure coupling in incompressible flows. The equation systems are solved by the successive overrelaxation method until all the residuals are less than 10^{-4}.

Four different grid arrangements, consisting of 6 million (coarse), 12 million (medium), 22 million (fine1) and 27 million (fine2) FV cells, are prepared to test grid sensitivity (Fig. 5). Most of the FV cells are hexahedra in the domain core. Toward the bottom, the cells are split into smaller hexahedra. The minimum grid sizes are 5.6 m, 4.2 m, 3.6 m and 3.3 m, respectively, for the cases with coarse, medium, fine1 and fine2 resolution. The grid sensitivity will be discussed in Sect. 3. In comparison to the recommendation by Franke et al. (2007) and Tominage et al. (2008), relatively coarse meshes are tested in the current study. This study focuses on the whole UBL instead of street-level ventilation, which might lessen the grid resolution requirements. In addition, it is aimed to foster a cost-effective grid resolution that can give reasonably accurate predictions. It will be useful for the future simulation of large-scale UBL flows.

3. Results and Discussion

3.1. Comparison of RANS and Wind Tunnel Results

In this section, selected vertical profiles of mean winds and turbulence obtained from the wind tunnel experiments and the RANS simulations are compared. The profiles are separated at $x = 153$ m apart (in full scale) in the streamwise direction. Reynolds decomposition is used to partition the mean (time-averaged) and fluctuating components. For instance, the velocity u_i is decomposed into its mean $\bar{u}_i$ and fluctuating u_i' components. Index notation is used where $i = 1$, 2 and 3 denote, respectively, the streamwise, spanwise and vertical components. The Reynolds stresses in the RNG $k-\varepsilon$ turbulence model are parameterized by the eddy-viscosity approach

$$\overline{u_i'u_j'} = -\nu_t\left(\frac{\partial \bar{u}_i}{\partial x_j} + \frac{\partial \bar{u}_j}{\partial x_i}\right) + \frac{2}{3}k\delta_{ij} \tag{5}$$

Here, ν_t is the kinematic eddy viscosity, x_i the coordinates and δ_{ij} the Kronecker delta.

Fig. 6 compares the mean $\bar{u}_i$ and turbulence $\overline{u_i'u_j'}$ properties obtained from the RANS simulations with the wind tunnel measurements along the five profiles (Fig. 3). The UBL thickness $\delta_{0.99}$ (defined by the 99% criteria of free-stream wind speed; Garratt 1994) and the corresponding mean wind speed $U|_{z=\delta_{0.99}}$ are used as the characteristic scales. In general, the results obtained from the RANS simulations and the wind tunnel experiments agree reasonably well. Their vertical variations and

magnitudes are comparable. The RANS results underestimate mildly the roof-level streamwise velocity $\bar{u}$ than do their wind tunnel counterparts. It is due to the underestimation of $\overline{u'w'}$ in the simulations, which implies weaker turbulent mixing, leading to a larger velocity gradient. The vertical flows are rather weak ($\overline{w} < U|_{z=\delta_{0.99}}$). Nonetheless, they are well captured by the RANS simulations. The roof-level streamwise fluctuating velocity $\overline{u'u'}^{1/2}$ calculated in the RANS simulation is much smaller than that measured in the wind tunnel experiments. It is also related to the discrepancy in $\overline{u'w'}$ near the roof level. Only mild differences are found among the RANS simulation results with different spatial resolutions. The comparison shows that even the case with coarse resolution can provide reasonably accurate results.

High-rise Buildings "A" (213 m) and "C" (255 m) are erected in the upstream region and beside the sampling profiles, respectively (Fig. 3). Their influence on the winds and turbulence downstream is notable. The turbulence generated in their wakes induce the upper peak of the $\overline{u'w'}$ profiles. These patterns are captured by the RANS simulations as well as the wind tunnel experiments. However, the eddy viscosity in the RNG $k-\varepsilon$ turbulence model is isotropic that cannot resolve the anisotropic fluctuating velocities $\overline{u_i'u_i'}^{1/2}$. This is an implicit limitation of RANS eddy-viscosity approach. The non-linear Reynolds stress model or LES is thus needed to simulate the anisotropic turbulence close to the buildings.

Besides, wiggles are observed downstream of the high-rise buildings in the RANS results. They are attributed to the local unsteadiness in response to the building-wake meandering that are less noticeable in the case with coarse grid resolution. Numerical dissipation increases with coarsening mesh that in turn suppresses those wiggles. In the following sections, all the CFD RANS results are based on the case with fine1 resolution.

3.2. Urban Boundary Layer

In Southerly wind conditions, an UBL is developed from Victoria Harbor to Mong Kok. In this section, the UBL development is characterized based on the RANS results. Fig. 7 depicts the contours of $\bar{u}$ and k on three selected vertical $(x-z)$ planes ($y = -210$ m, 0 m, and 210 m). It illustrates that the UBL thickness in downtown Mong Kok region is about 350 m (the estimate of UBL thickness will be discussed in Sect. 3.3.2). Elongated wakes, whose streamwise extent is over 2 km, are found behind the few high-rise buildings (with height $>$ 150 m), occupying almost the whole UBL. The TKE in the wakes elevates to $0.02U_0^2$ that is attributed to the substantial shear formed behind the high-rise buildings. These results signify the importance of high-rise buildings in UBL structure that are consistent with previous findings (Flaherty et al., 2007; Xie and Castro, 2009; Moon et al., 2014; Hertwig et al., 2019).

Figure 8 depicts the contours of $\bar{u}$ and k on the horizontal $(x-y)$ planes at different elevations. As expected, the UBL flows over real urban surfaces are highly heterogeneous. At the 50-m level, the flows slow down whose TKE sinks within the urban canopies because of the sheltering and recirculations in dense built environment. These flow patterns are analogous to the skimming flows originally proposed for idealized urban canopies (Oke, 1988). At the 100-m level, where is already higher than most of the buildings, several building wakes are developed in which k increases locally in response to the elevated shear along the edges of building wakes. At higher levels $z = 150$ m, 200 m and 250 m, the wakes are elongated with elevated k because of the high wind speeds. Some of the wakes have streamwise extent over 2 km and spanwise coverage of 200 m to 300 m.

The momentum transport mechanism above real urban surfaces is different from that obtained from idealized building blocks (Cheng and Porté-Agel, 2015, 2016). In those cases, k and $\left|\overline{u'w'}\right|$ were found peaked in the lower UBL just above the idealized, uniform cube arrays. Under this circumstance, the urban canopies indirectly promote the UBL growth by dragging momentum from the free-stream flows aloft. Above real urban surfaces, on the contrary, individual high-rise buildings affect the flows extensively that collectively modify the UBL turbulence characteristics. This makes a key difference in the flow structures between real and idealized urban

morphology. The consideration of realistic urban geometries is thus needed to properly parameterize UBL flows in line with previous studies (Kanda et al., 2013; Ramirez et al., 2018; Theeuwes et al., 2019).

3.2.1. Locally-averaged profiles

In order to quantitatively investigate the UBL growth, horizontally-averaged profiles (within a zone) of $\langle \bar{u} \rangle$, $\langle k \rangle$ and $\langle \overline{u'w'} \rangle$ are considered. The averaging areas are located within $-225\,m < y < 225\ m$ and $300\,m < x < 3{,}900\,m$ (Fig. 9). The samples are uniformly distributed on the $x - y$ (horizontal) plane that are interpolated from the RANS results with a spatial resolution of $x = y = 30\,m$. This corresponds to a total of $16 \times 120 = 1{,}920$ vertical profiles. Within the urban canopy, extrinsic spatial averages (averages over the total volume rather than the fluid volume) is used (Castro, 2017). As the UBL is developing in the streamwise (x) direction, the region concerned is sub-divided into 12 small zones each with sizes $300\,m \times 350\,m$ (Fig. 9). It was found that, for different urban surfaces, a representative building packing density can be obtained for horizontal length scales longer than 250 m (Oke et al., 2017).

The locally-averaged profiles of mean streamwise velocity $\langle \bar{u} \rangle$, TKE $\langle k \rangle$ and momentum $\langle \overline{u'w'} \rangle$ are depicted in Fig. 10 together with the evolution of UBL

thickness $\delta_{0.99}$. Alike the previous discussion in Sect. 3.2, $\delta_{0.99} \approx 350$ m is found at $x \approx 4$ km downstream of the coastal line. It is found that $\langle \bar{u} \rangle$, $\langle k \rangle$ and $\langle \overline{u'w'} \rangle$ mostly diminish below $z = 50$ m because of the building blockage and recirculating flows. The peaks of $\langle k \rangle$ and $\langle \overline{u'w'} \rangle$ are associated with high-rise buildings. For instance, two sharp peaks of $\langle k \rangle$ and $\langle \overline{u'w'} \rangle$ are observed for 1,200 m $\leq x \leq$ 1,500 m that are induced by Buildings "A" and "B" (Fig. 10). Other peaks ($z \approx 255$ m) of $\langle k \rangle$ and $\langle \overline{u'w'} \rangle$ are associated with Building "C" for $x \geq$ 3,300 m. These results are consistent with those of Xie et al. (2008) and Xie and Castro (2009), demonstrating the unique roles of high-rise buildings in UBL development.

3.3. Urban Canopy Model (UCM) Parameters

The RANS results are further analyzed to parameterize urban canopy flows using the traditional one-dimensional (1D) UCM (Raupach and Shaw, 1982; Finnigan, 2000; Coceal and Belcher, 2005). The steady-state 1D simplified spatio-temporally averaged momentum equation of flows within the urban canopy reads

$$\frac{\partial \langle p \rangle}{\partial x} = -\frac{\partial \langle \overline{u'w'} \rangle}{\partial z} - \frac{\partial \langle \tilde{u}\tilde{w} \rangle}{\partial z} - D_x \tag{6}$$

where $\tilde{u} = \bar{u} - \langle \bar{u} \rangle$, $\langle \tilde{u}\tilde{w} \rangle$ the dispersive stress, D_x the effective drag exerted by the urban surfaces on the flows and p the kinematic pressure. Parameterizations of $\langle \overline{u'w'} \rangle$, $\langle \tilde{u}\tilde{w} \rangle$ and D_x are essential to UCM. Among others, the stresses can be parametrized

by the mixing length l_m formulation (Macdonald, 2000; Coceal and Belcher, 2004) as

$$-[\langle\overline{u'w'}\rangle + \langle\tilde{u}\tilde{w}\rangle] = \left(l_m(z)\frac{\partial\langle\bar{u}\rangle}{\partial z}\right)^2 \quad (7)$$

On the left-hand side of Eq. (7), both the turbulent $\langle\overline{u'w'}\rangle$ and the dispersive $\langle\tilde{u}\tilde{w}\rangle$ stresses are included. Dispersive stress is not commonly considered in the literature (Castro, 2017) whose calculation for real urban surfaces is very limited (Giometto et al., 2016).

3.3.1. Mean stress, turbulent stress and dispersive stress

Figure 11 depicts the locally-averaged vertical profiles of the mean stress $\langle\bar{u}\rangle\langle\bar{w}\rangle$, turbulent stress $\langle\overline{u'w'}\rangle$ and dispersive stress $\langle\tilde{u}\tilde{w}\rangle$ in different zones. Since the (explicitly resolved) buildings significantly slow down the near ground flows, elevated mean stress is found near the harbor-to-urban transition (coastline) with $\langle\bar{u}\rangle\langle\bar{w}\rangle \approx 0.04U_0^2$ at $z \approx 100$ m (Fig. 11a). While the flows are adjusting to the urban surfaces, the mean-stress magnitude decreases gradually further downstream. The current RANS results reveal that the mean stress is smaller than the Reynolds stress at the region 3 km downstream of the coastline. Peaks associated with the high-rise buildings are also found in the mean stress profiles (Fig. 11a).

Fully adjusted pattern of $\langle\overline{u'w'}\rangle$ is found in the downstream regions (after Zone "7") located at 2 km downstream of the coastline (Fig. 11b). In these regions, $\left|\langle\overline{u'w'}\rangle\right|$

is peaked at $z = 200$ m with a value $\approx 3 \times 10^{-3} U_0^2$. The shape of the vertical profile is similar to that of idealized urban canopies with which $\left|\langle \overline{u'w'} \rangle\right|$ is peaked at the height of the building blocks (Cheng and Porté-Agel, 2015). Alike the Reynolds stress, the dispersive stress is found to attain an adjusted profile for $x \geq 2$ km. The magnitudes of the Reynolds stress and the dispersive stress are comparable for $z \leq 100$ m below the majority urban canopy level. This is consistent with the LES results of Giometto et al. (2016) who studied the flows in the city of Basel, Switzerland. At higher levels ($100 \text{ m} < z < 300 \text{ m}$), the Reynolds stress is much larger than the dispersive stress. For instance, at $z = 200$ m, the magnitude of the dispersive stress is about 20% to 30% of the Reynolds stress. Nonetheless, the dispersive stress is non-negligible.

3.3.2. Mixing length and effective drag

Fig. 12 displays the vertical profiles of mixing length l_m (Eq. 7) in Zones 10, 11 and 12 located within $3 \text{ km} \leq x \leq 3.9 \text{ km}$. Horizontally homogeneous flows are usually assumed in 1D UCMs. Although real urban surfaces are not horizontally homogeneous, l_m shows consistent behaviors among different zones (Fig. 12). This confirms that, after performing the horizontal averaging, homogeneity of the stress profiles is observed for the downstream zones where the flow is already adjusted to the

urban surface. In these zones, the mixing length calculated with (denoted as l_m) and without (denoted as l'_m) the dispersive stress is compared in Fig. 12. They are consistent with the analysis of Castro (2017) in which the dispersive stress does not change much the mixing length profile. A slight increase in the local maximum (less than 20%) at $z = 200$ m is observed.

Different UBL sublayers can be identified based on l_m. Firstly, $\partial l_m/\partial z \approx 0.4$ for $350 \text{ m} \leq z \leq 400$ m that is in line with the Prandtl hypothesis in the surface layer of TBL flows (Garratt, 1994). This layer can be identified as the inertial sublayer (ISL) above the urban canopy. Below the ISL is the urban roughness sublayer (URSL). At the three different streamwise locations (Fig. 12), the URSL tops at $z \approx 350$ m that grows further in the streamwise direction. Note that the ISL identified here is above the UBL defined earlier (based on the criteria of wind speed equals 99% of the freestream level; Fig. 10). This apparently contradicts the UBL definition that, above the UBL, the flows are characterized by the upstream conditions (Ferziger and Peric, 2002). It is probably because the adopted UBL definition is only a crude estimate. It actually identifies the URSL top instead of the UBL in the current case. Therefore, a more precise physical definition (than the criteria of 99% free-stream velocity) is necessary for UBL identification.

Fig. 12 also shows that the URSL can be further divided into two layers. Near the

surface ($z \leq 100$ m), where the urban canopy is occupied by dense, short buildings, l_m can be considered uniform with height (apart from some minor, random fluctuations). Above 100 m, l_m depends clearly on height whose maximum locates at $z \approx 200$ m (at about the mid-level of the upper layer). In line with the previous discussion of the Reynolds stress profiles (Section 3.3.1), the l_m profiles in this layer are similar to those of idealized building blocks (Coceal et al., 2006; Cheng and Porté-Agel, 2015; Castro, 2017). The mixing length l_m is normalized by the height of Building "C" (H_c = 255.1 m). The maximum l_m/H_c is about 0.1 which is smaller than that of uniform building blocks (Coceal et al., 2006; Kono et al., 2010; Cheng and Porté-Agel, 2015; Castro, 2017). It is noteworthy that, in the lower layer ($z \leq 100$ m), l_m should be normalized using the characteristic length scale of the shorter buildings instead of the taller ones.

The effective drag D_x (Eq. 6) exerted by the buildings on the flows is another important parameter in UCM. Since the surface geometry of Kowloon Peninsula is complicated, using the traditional method to calculate the drag of all the buildings is impractical. Instead, D_x is estimated indirectly based on the force balance in Eq. 6. It is noteworthy that the urban surfaces in the enclosed regions (Fig. 9) is heterogeneous, further validations of the flows and turbulence within deep urban canopies are thus needed. Nevertheless, with well awareness of the potential uncertainties, most of the

drag is exerted below 100 m as shown by the profiles of the estimated normalized effective drag (Fig. 12 b). This can be explained by the much higher density of the shorter buildings than their high-rise counterparts. From 50 m to 100 m, the effective drag decreases with increasing height that qualitatively agrees with that in previous studies based on idealized urban canopies (Cheng and Castro, 2002; Santiago et al., 2008; Leonardi and Castro, 2010; Castro, 2017). Below 50 m, D_x is not shown in Fig. 12 (b) since recirculating flows dominate.

4. Conclusions

Most existing studies characterized the urban roughness sublayer (URSL) have only based on idealized urban surfaces represented by 2D street canyons or 3D block arrays. The effects of heterogeneous real urban surfaces on URSL transport is still not well understood. Under this circumstance, this paper applies novel wind tunnel experiment and the steady-state incompressible RANS methods to examine the urban boundary layer (UBL) development above Kowloon Peninsula, HKSAR in neutral thermal stratification.

The RANS simulation results are first validated against the wind tunnel measurements. The grid independence of the RANS results is evaluated using four different grid arrangements. Reasonably well predictions are found for the mean winds

and turbulence, though the limitations of RANS approach are unveiled. The anisotropic turbulence close to the urban surfaces is merely resolved numerically.

Afterward, the RANS results are analyzed to characterize the UBL. In general, the UBL structure is significantly influenced by the presence of high-rise buildings. In particular, wakes extending to 2 ~ 3 km downstream of the high-rise buildings are found in the RANS results. By calculating the local-spatially-averaged profiles of $\bar{u}$, k, and $\overline{u'w'}$, wakes patterns and peaks of $\langle k \rangle$ and $\langle \overline{u'w'} \rangle$ associated with individual high-rise buildings are observed. These findings highlight the importance of sparse, high-rise buildings to the UBL dynamics.

In attempt to enrich the turbulence parameterizations of urban canopy flows, several important quantities of the traditional 1D urban canopy model (UCM), including the mixing length l_m, the effective drag D_x and the dispersive stress within and above the urban canopy, are examined. Based on the RANS results (in the downstream region where the flows are already adjusted to the urban surfaces), it is found that the URSL can be divided into the upper (approximately $100\ \text{m} \leq z \leq 350\ \text{m}$) and lower (about $z \leq 100\ \text{m}$) URSLs, depending on the majority building height. In the upper URSL, the flows are mainly governed by the high-rise buildings, and l_m is peaked approximately at the mid-height. In the lower URSL, the dense, shorter buildings tremendously weaken the flows that results in a smaller, more uniform

(but fluctuating) l_m. On the other hand, the magnitude of the dispersive stress is comparable to the Reynolds stress in the lower URSL but is smaller than its upper URSL counterpart (< 30%). The drag D_x, which is estimated based on force balance (Eq. 6), is mostly exerted in the lower URSL due to the dense, shorter buildings. By dividing the URSL into the aforementioned two layers, the current results demonstrate the potential to develop a universal UCM for complex, real urban canopies.

This paper considered a case study of the neutral UBL above Kowloon urban morphology. In the future studies, investigation on the effects of thermal stratifications and different urban surface types will be attempted. In addition, large-eddy simulation (LES) will be used to study the unsteady and highly anisotropic turbulent flows in URSL.

References

Antoniou N, Montazeri H, Wigo H, Neophytou MKA, Blocken B, Sandberg M (2017). CFD and wind-tunnel analysis of outdoor ventilation in a real compact heterogeneous urban area: Evaluation using “air delay". Building and Environment 126, 355-372.

Barlow J, Belcher SE (2002). A wind tunnel model for quantifying fluxes in the urban boundary layer. Boundary-Layer Meteorology 104, 131-150.

Barlow J, Best M, Bohnenstengel SI, Clark P, Grimmond S, Lean H, et, al. (2017). Developing a research strategy to better understand, observe and simulate urban atmospheric processes at kilometre to sub-kilometre scales. Bulletin of the American Meteorological Society 98, ES261-ES262. doi:https://doi.org/10.1175/BAMS-D-17-0106.1.

Belcher SE, Coceal O, Goulart EV, Rudd AC, Robins AG (2015). Processes controlling atmospheric dispersion through city centres. Journal of Fluid Mechanics 763, 51-81.

Blocken B, Janssen WD, van Hooff T (2012). CFD simulation for pedestrian wind comfort and wind safety in urban areas: General decision framework and case study for the Eindhoven university campus. Environmental Modelling & Software 30, 15-34.

Bruun H, 1971. Interpretation of a hot wire signal using a universal calibration law. Journal of Physics E: Scientific Instruments 4, 225.

Castro IP, 2012. Effects of wall heating on flow characteristics in a street canyon. Boundary-Layer Meteorology 142, 443-467.

Castro IP, 2017. Are urban-canopy velocity profiles exponential? Boundary-Layer Meteorology 164, 337-351.

Castro IP, Cheng H, Reynolds R (2006). Turbulence over urban-type roughness: deductions from wind-tunnel measurements. Boundary-Layer Meteorology 118, 109-131.

Cheng H, Castro I (2002). Near wall flow over urban-like roughness. Boundary-Layer Meteorology 104, 229-259.

Cheng WC, Liu CH (2011). Large-eddy simulation of flow and pollutant transports in and above two-dimensional idealized street canyons. Boundary-Layer Meteorology 139, 411-437.

Cheng WC, Porté-Agel F (2015). Adjustment of turbulent boundary-layer flow to idealized urban surfaces: a large-eddy simulation study. Boundary-Layer Meteorology 155, 249-270.

Cheng WC, Porté-Agel F (2016). Large-eddy simulation of flow and scalar dispersion in rural-to-urban transition regions. International Journal of Heat and Fluid Flow 60, 481 47-60.

Coceal O, Belcher SE (2004). A canopy model of mean winds through urban areas. Quarterly Journal of the Royal Meteorological Society 130, 1349-1372.

Coceal O, Belcher SE (2005). Mean winds through an inhomogeneous urban canopy. Boundary-Layer Meteorology 115, 47-68.

Coceal Z, Thomas TG, Castro IP, Belcher SE (2006). Mean flow and turbulence statistics over groups of urban-like cubical obstacles. Boundary-Layer Meteorology 121, 491-519.

Efthimiou GC, Berbekar E, Harms F, Bartzis JG, Leitl B (2015). Prediction of high concentrations and concentration distribution of a continuous point source release in a semi-idealized urban canopy using CFD-RANS modeling. Atmospheric Environment 100, 48-56.

Ferziger JH, Peric M (2002). Computational Methods for Fluid Dynamics 3rd Edition. Springer. 426 pp.

Finnigan JJ (2000). Turbulence in plant canopies. Annual Review of Fluid Mechanics 496 32, 519-571.

Flaherty J, Stock D, Lamb B (2007). Computational fluid dynamic simulations of plume dispersion in urban Oklahoma city. Journal of Applied Meteorology and Climatology 46, 2110-2126.

Franke J, Hellsten A, Sckünzen H, Carissimo B (2007). Best practice guideline for the

CFD simulation of flows in the urban environment. COST Office, Brussels, ISBN 3-00-018312-4.

Gao Z, Bresson R, Qu Y, Milliez M, Munck C, Carissimo B (2018). High resolution unsteady RANS simulation of wind, thermal effects and pollution dispersion for studying urban renewal scenarios in a neighborhood of Toulouse. Urban Climate 23, 114-130.

Garratt JR (1994). The Atmospheric Boundary Layer 3rd edition. Cambridge University Press. 336 pp.

Giometto MG, Christen A, Meneveau C, Fang J, Krafczyk M, Parlange MB (2016). Spatial characteristics of roughness sublayer mean flow and turbulence over a realistic urban surface. Boundary-Layer Meteorology 160, 425-452.

Goulart EV, Coceal O, Belcher SE (2018). Dispersion of a passive scalar within and above an urban street network. Boundary-Layer Meteorology 166, 351-366.

Gousseau P, Blocken B, Stathopoulos T, van Heijst GJF (2015). Near-field pollutant dispersion in an actual urban area: analysis of the mass transport mechanism by high-resolution large eddy simulations. Computers & Fluids 114, 151-162.

Gousseau P, Blocken B, Stathopoulos T, van Heijst GJF (2011). CFD simulation of near-field pollutant dispersion on a high-resolution grid: A case study by LES and RANS for a building group in downtown Montreal. Atmospheric Environment 45, 428-438.

Grimmond CSB, Oke TR (1999). Aerodynamic properties of urban areas derived from analysis of surface form. Journal of Applied Meteorology 38, 1262-1291.

Hamlyn D, Hilderman T, Britter R (2007). A simple network approach to modelling dispersion among large groups of obstacles. Atmospheric Environment 41, 5848-5862.

Hang J, Li Y (2010). Wind conditions in idealized building clusters - macroscopic simulations using a porous turbulence model. Boundary-Layer Meteorology 136(1), 129-159.

Hang J, Li Y (2012). Macroscopic simulations of turbulent flows through high-rise

building arrays using a porous turbulence model. Building and Environment 49, 41-54.

Hanna SR, Brown MJ, Camelli FE, Chan ST, Coirier WJ, Hansen OR, Huber AH, Kim S, Reynolds RM (2006). Detailed simulations of atmospheric flow and dispersion in downtown Manhattan: an application of five computational fluid dynamics models. Bulletin of the American Meteorological Society 87(12), 1713-1726.

Hertwig D, Efthimiou GC, Bartzis JG, Leitl B (2012). CFD-RANS model validation of turbulent flow in a semi-idealized urban canopy. Journal of Wind Engineering & Industrial Aerodynamics 11, 61-72.

Hertwig D, Gough LL, Grimmond S, Barlow JF, Kent CW, Lin WE, Robins AG, Hayden P (2019). Wake characteristics of tall buildings in a realistic urban canopy. Boundary-Layer Meteorology 172, 239-270.

Hong Kong Lands Department (2018). Hong Kong Map Service, Survey and Mapping Offce, Lands Deparment, HKSAR. https://www.hkmapservice.gov.hk.

Kanda M, Inagaki A, Miyamoto T, Gryschka M, Raasch S (2013). A new aerodynamic parametrization for real urban surfaces. Boundary-Layer Meteorology 148, 357-377.

Kono T, Tamura T, Ashie Y (2010). Numerical investigations of mean winds within canopies of regularly arrayed cubical buildings under neutral stability conditions. Boundary-Layer Meteorology 134, 131-155.

Leonardi S, Castro IP (2010). Channel flow over large cube roughness: a direct numerical simulation study. Journal of Fluid Mechanics 651, 519-539.

Letzel MO, Krane M, Raasch S (2008). High resolution urban large-eddy simulation studies from street canyon to neighbourhood scale. Atmospheric Environment 42, 8770-8784.

Leung KK, Liu CH (2012). Local mass transfer coefficient over idealized two-dimensional urban street canyons. International Journal of Environment and Pollution 50, 75-82.

Leung KK, Liu CH, Wong CCC, Lo JCY, Ng GCT (2012). On the study of ventilation and pollutant removal over idealized two-dimensional urban street canyons. Building

Simulation 5, 359-369.

Macdonald RW (2000). Modelling the mean velocity profile in the urban canopy layer. Boundary-Layer Meteorology 97, 25-45.

Mo Z, Liu CH (2018). Wind tunnel measurements of pollutant plume dispersion over hypothetical urban areas. Building and Environment 132, 357-366.

Moon K, Hwang JM, Kim BG, Lee C, Choi J (2014). Large-eddy simulation of turbulent flow and dispersion over a complex urban street canyon. Environmental Fluid Mechanics 14, 1381-1403.

Neophytou M, Gowardhan A, Brown M (2011). An inter-comparison of three urban wind models using Oklahoma City Joint Urban 2003 wind field measurements. Journal of Wind Engineering & Industrial Aerodynamics 99, 357-368.

Ng E, Yuan C, Chen L, Ren C, Fung JCH (2011). Improving the wind environment in high-density cities by understanding urban morphology and surface roughness: A study in Hong Kong. Landscape Urban Plan 101(1), 59-74.

Nozu T, Tamura T (2012). LES of turbulent wind and gas dispersion in a city. Journal of Wind Engineering & Industrial Aerodynamics 104-106, 492-499.

Oke TR (1988). Boundary Layer Climates 2nd edition. Routledge. 464 pp.

Oke TR, Mills G, Christen A, Voogt JA (2017). Urban Climates. Cambridge University Press. 519 pp.

OpenFOAM (2020). User Guide. OpenFOAM.

Ramirez N, Afshari A, Norford L (2018). Validation of simplified urban canopy aerodynamic parametrizations using a numerical simulation of an actual downtown area. Boundary-Layer Meteorology 168, 155-187.

Raupach MR (1992). Drag and drag partition on rough surfaces. Boundary-Layer Meteorology 60, 375-395.

Raupach MR, Shaw RH (1982). Averaging procedures for flow within vegetation

canopies. Boundary-Layer Meteorology 22, 79-90.

Ricci A, Burlando M, Freda A, Repetto MP (2017). Wind tunnel measurements of the urban boundary layer development over a historical district in Italy. Building and Environment 111, 192-206.

Santiago JL, Coceal O, Martilli A, Belcher SE (2008). Variation of the sectional drag coefficient of a group of buildings with packing density. Boundary-Layer Meteorology 128, 445-457.

Spalding DB (1961). A single formula for the “Law of the wall”. Journal of Applied Mechanics 28, 455-458.

Theeuwes NE, Ronda RJ, Harman IN, Christen A, Grimmond CSB (2019). Parametrizing horizontally-averaged wind and temperature profiles in the urban roughness sublayer. Boundary-Layer Meteorology 173, 321-348.

Tolias IC, Koutsourakis N, Hertwig D, Efthimiou GC, Venetansos AG, Bartzis JG (2018). Large eddy simulation study on the structure of turbulent flow in a complex city. Journal of Wind Engineering & Industrial Aerodynamics 177, 101-116.

Tominaga Y, Sato Y, Sadohara S (2015). CFD simulations of the effect of evaporative cooling from water bodies in a micro-scale urban environment: validation and application studies. Sustainable Cities and Society 19, 259-270.

Tominage Y, Mochida A, Yoshie R, Kataoka H, Nozu T, Yoshikawa M, Shirasawa T (2008). AIJ guidelines for practical applications of CFD to pedestrian wind environment around buildings. Journal of Wind Engineering & Industrial Aerodynamics 96, 1749-1761.

Toparlar Y, Blockeni B, Vos P, van Heijst GJF, Janssen WD, van Hoof T, Montazeri H, Timmermans HJP (2015). CFD simulation and validation of urban microclimate: A case study for Bergpolder Zuid, Rotterdam. Building and Environment 83, 79-90.

Wang W, Ng E (2018). Air ventilation assessment under unstable atmospheric stratification – a comparative study for Hong Kong. Building and Environment 130, 1-13.

Wong MS, Nichol JE, To PH, Wang J (2010). A simple method for designation of urban ventilation corridors and its application to urban heat island analysis. Building and Environment 45, 1880-1889.

Wu Z, Liu CH (2018). Budget analysis for reactive plume transport over idealised urban areas. Geoscience Letters 5, 5-19.

Xie ZT, Castro IP (2009). Large-eddy simulation for flow and dispersion in urban streets. Atmospheric Environment 43, 2174-2185.

Xie ZT, Coceal O, Castro IP (2008). Large-eddy simulation of flows over random urban-like obstacles. Boundary-Layer Meteorology 129, 1-23.

Yakhot V, Orszag SA (1992). Development of turbulence models for shear flows by a double expansion technique. Physics of Fluids A: Fluid Dynamics 4, 1510-1520.

Yang XIA, Meneveau C (2016). Large eddy simulations and parameterisation of roughness element orientation and flow direction effects in rough wall boundary layers. Journal of Turbulence 17, 1072-1085.

Yuan C, Ng E, Norford LK (2014). Improving air quality in high-density cities by understanding the relationship between air pollutant dispersion and urban morphologies. Building and Environment 71, 245-258.

Zhai Z, Zhang Z, Zhang W, Chen Q (2007). Evaluation of various turbulence models in predicting airflow and turbulence in enclosed environments by CFD: Part 1-summary of prevalent turbulence models. HVAC&R Research 13, 853-870.

Figure Captions

Figure 1: (a) Geographic map (Hong Kong Lands Department, 2018) and (b) satellite image of Kowloon Peninsula, HKSAR. The red rectangle outlines the urban areas being considered in this paper.

Figure 2: Building height distribution. Not shown are five high-rise buildings which are over 150 m.

Figure 3: Reduced-scale (1:1; 500) 3D-printing urban model in the laboratory wind tunnel experiments. Also shown is the sampling probe of CT HWA.

Figure 4: Computational domain for the CFD RANS models.

Figure 5: CFD meshes of (a) coarse, (b) medium and (c) fine spatial resolutions.

Figure 6: Comparisons between the wind tunnel measurements and RANS modeling results of (a) $\bar{u}$, (b) $\bar{w}$, (c) $\overline{u'w'}$ together with (d) $\overline{u'u'}^{1/2}$ and $\overline{w'w'}^{1/2}$ along the five profiles: (i) I, (ii) II, (iii) III, (iv) IV, (v) V as labeled in Fig. 3.

Figure 7: UBL development and contours of (a) mean streamwise velocity $\bar{u}$ and (b) TKE k on selected vertical $(x-z)$ planes.

Figure 8: Contours of (a) mean streamwise velocity $\bar{u}$ and (b) TKE k on selected horizontal $(x-y)$ planes.

Figure 9: Zones (enclosed by the 12 red boxes) divided for horizontally spatial-average analysis.

Figure 10: Vertical profiles of horizontal and time averaged properties (a) $\langle\bar{u}\rangle$, (b) $\langle\bar{k}\rangle$ and (c) $\langle\overline{u'w'}\rangle$.

Figure 11: (a) Horizontal and time averaged mean $\langle\bar{u}\rangle\langle\bar{w}\rangle$, turbulent $\langle\overline{u'w'}\rangle$ and dispersive $\langle\tilde{u}\tilde{w}\rangle$ stresses in different zones (labeled by the red number according to those in Fig. 9. (b) Detailed patterns of turbulent $\langle\overline{u'w'}\rangle$ and dispersive $\langle\tilde{u}\tilde{w}\rangle$ stresses plotted in zoomed scale.

Figure 12: (a) Mixing Length l_m (without dispersive stress), l'_m (with dispersive

stress) and (b) effective drag D_x in different zones (labeled by the red number according to those in Fig. 9).

Figures

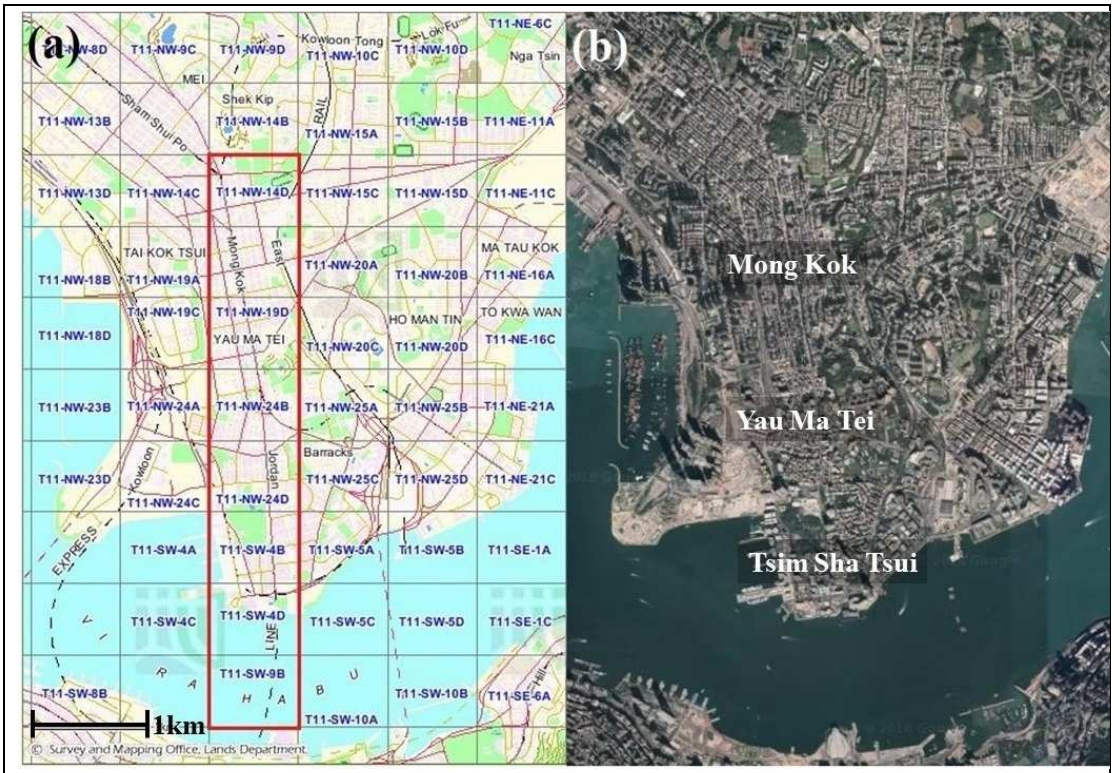

Figure 1: (a) Geographic map (Hong Kong Lands Department, 2018) and (b) satellite image of Kowloon Peninsula, HKSAR. The red rectangle outlines the urban areas being considered in this paper.

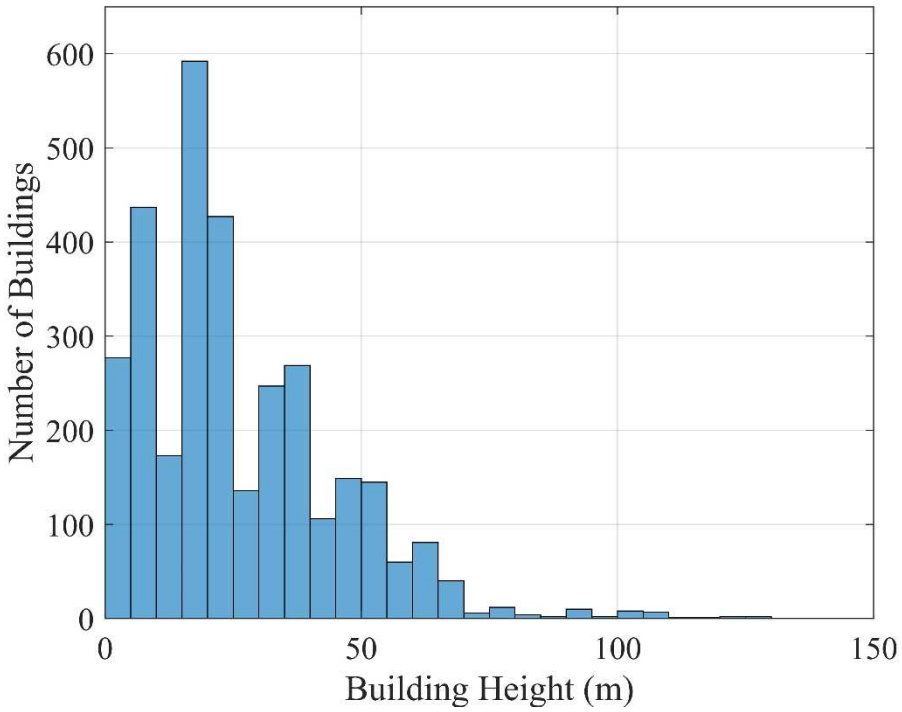

Figure 2: Building height distribution. Not shown are five high-rise buildings which are over 150 m.

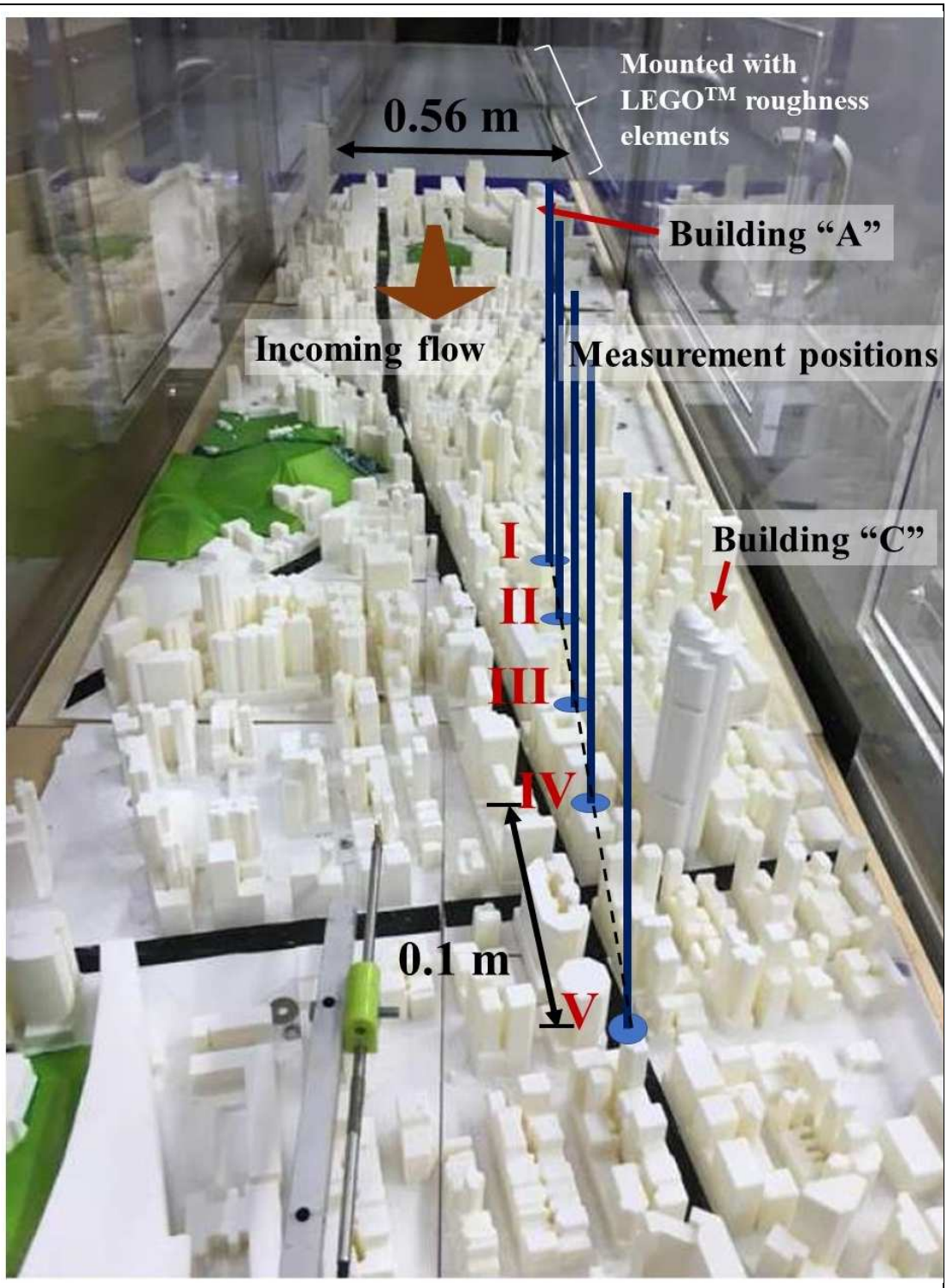

Figure 3: Reduced-scale (1:1; 500) 3D-printing urban model in the laboratory wind tunnel experiments. Also shown is the sampling probe of CT HWA.

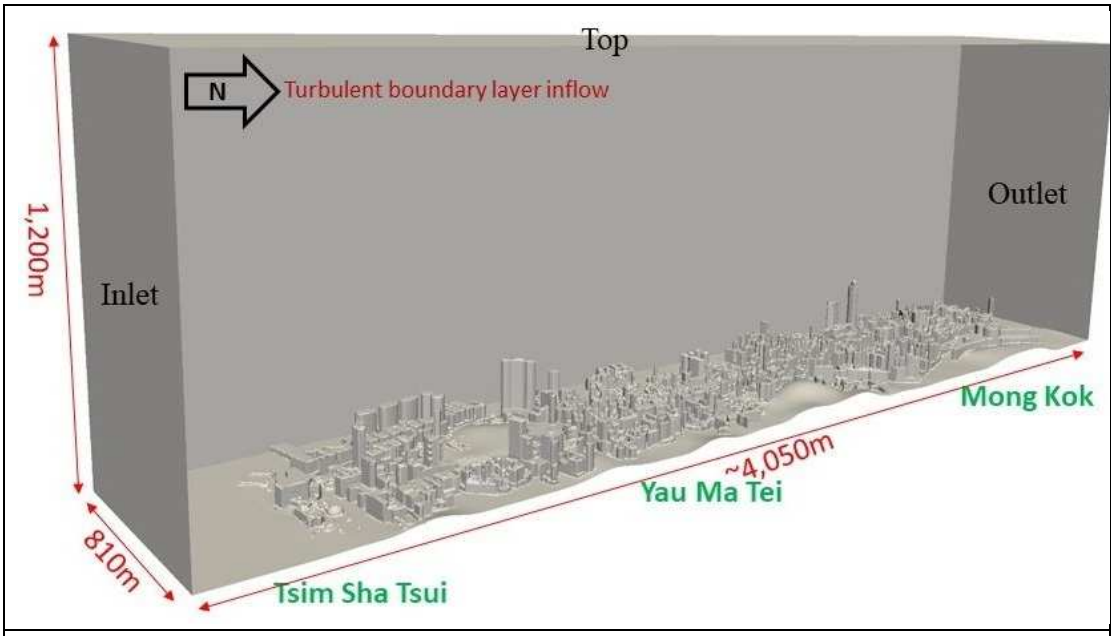

Figure 4: Computational domain for the CFD RANS models.

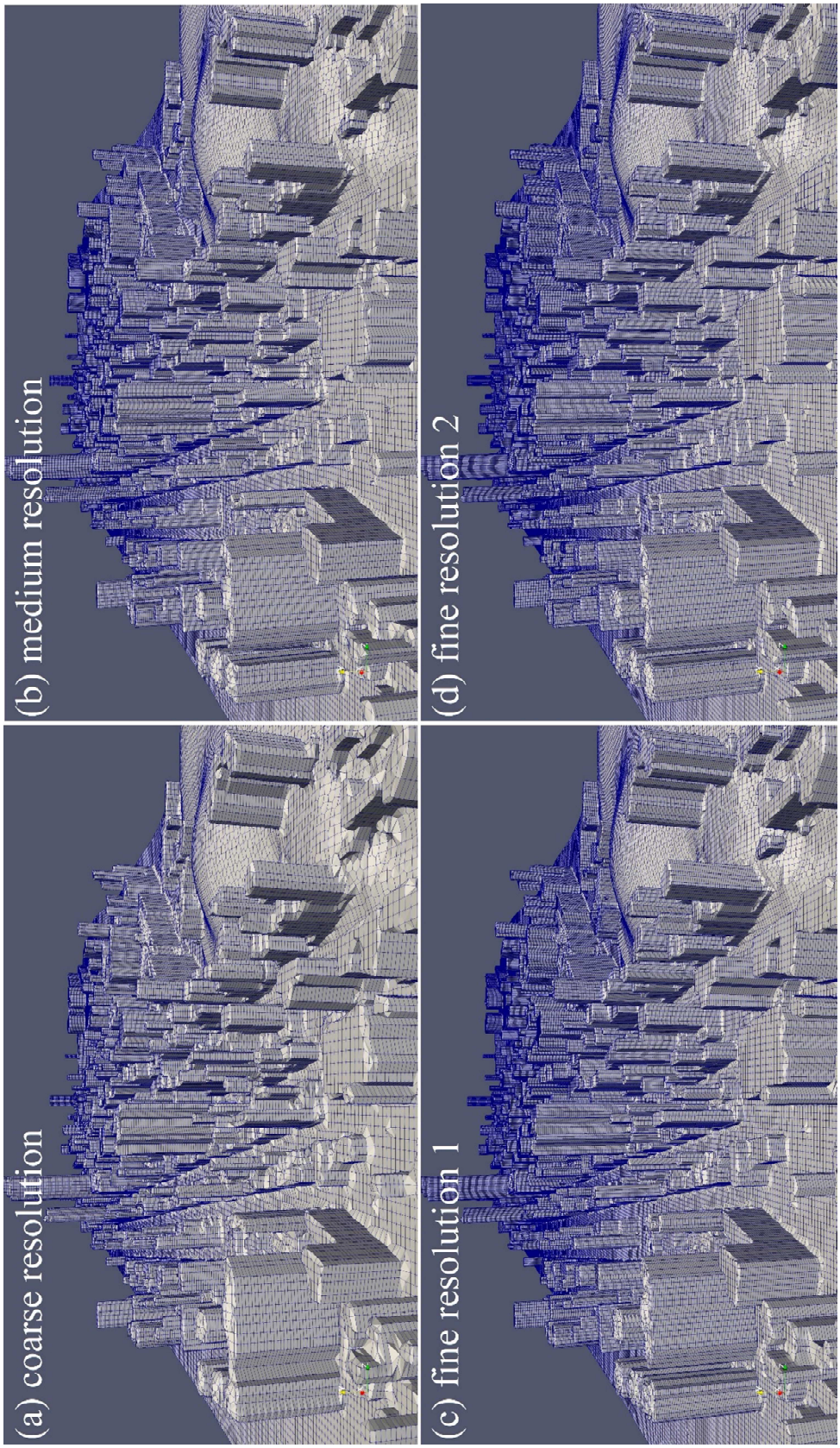

Figure 5: CFD meshes of (a) coarse, (b) medium and (c) fine1 and (d) fine2 spatial resolutions.

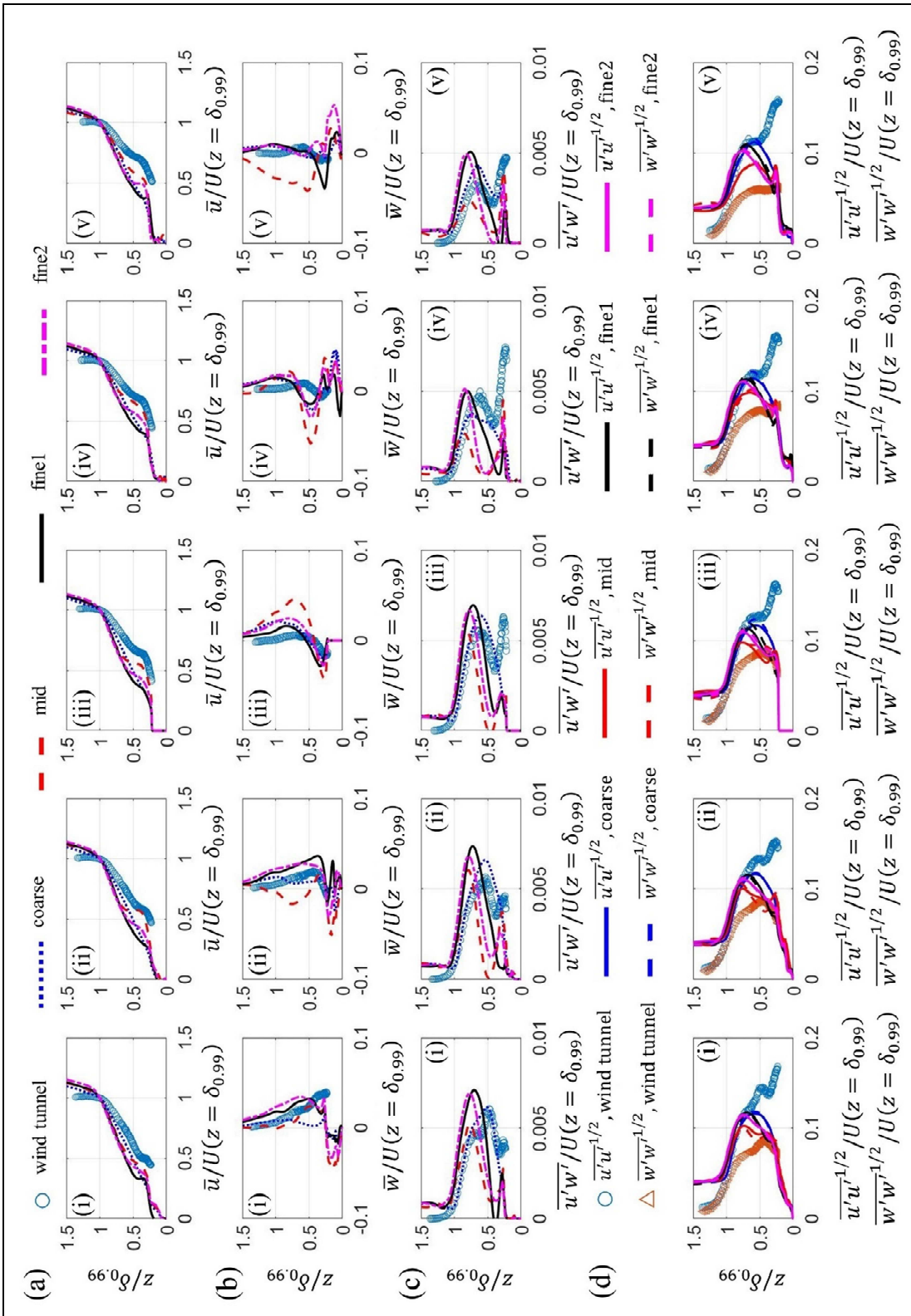

Figure 6: Comparisons between the wind tunnel measurements and RANS modeling results of (a) $\bar{u}$, (b) $\bar{w}$, (c) $\overline{u'w'}$ together with (d) $\overline{u'u'}^{1/2}$ and $\overline{w'w'}^{1/2}$ along the five profiles: (i) I, (ii) II, (iii) III, (iv) IV, (v) V as labeled in Fig. 3.

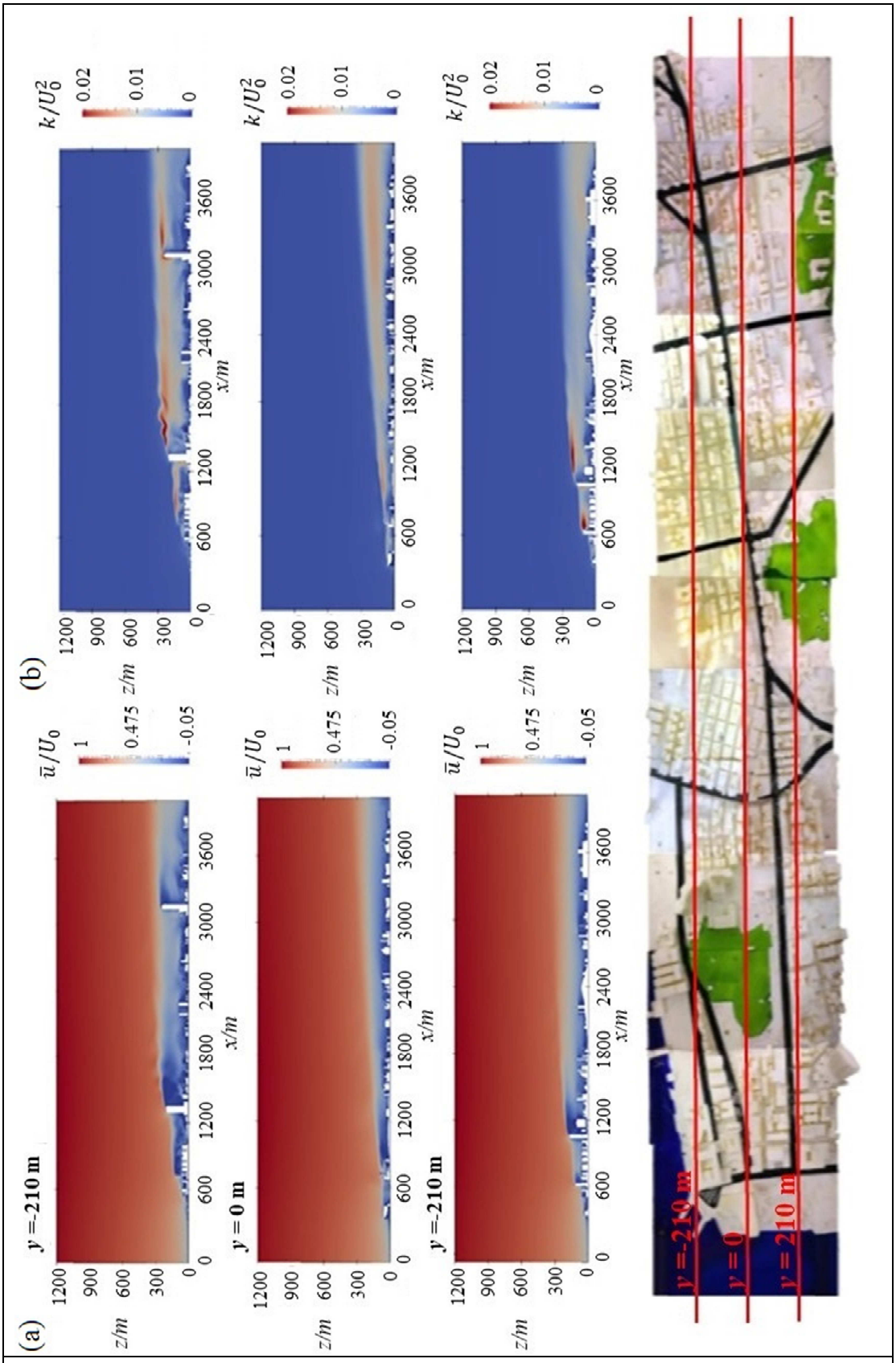

Figure 7: UBL development and contours of (a) mean streamwise velocity $\bar{u}$ and (b) TKE k on selected vertical $(x-z)$ planes.

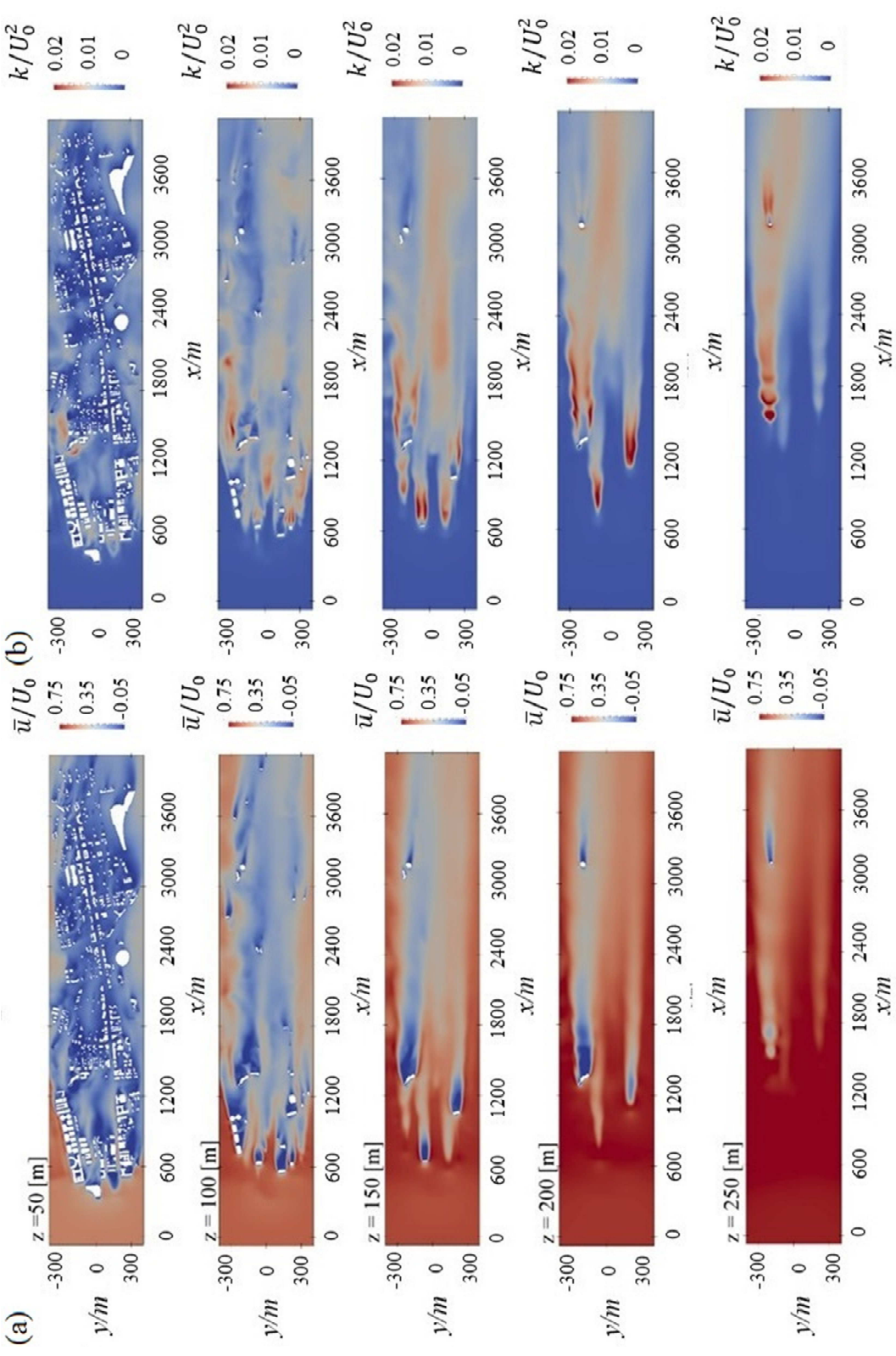

Figure 8: Contours of (a) mean streamwise velocity $\bar{u}$ and (b) TKE k on selected horizontal $(x-y)$ planes.

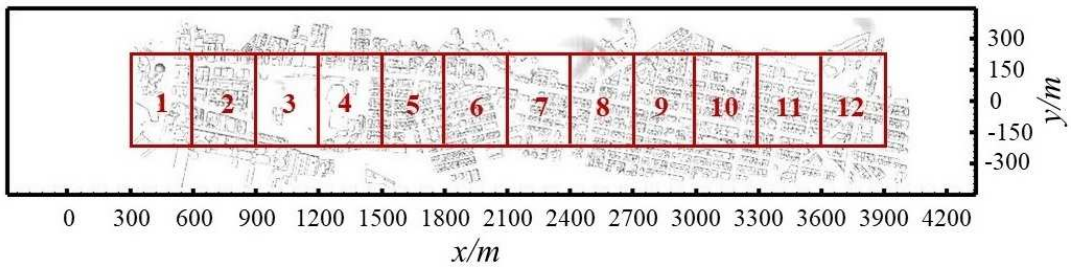

Figure 9: Zones (enclosed by the 12 red boxes) divided for horizontally spatial-average analysis.

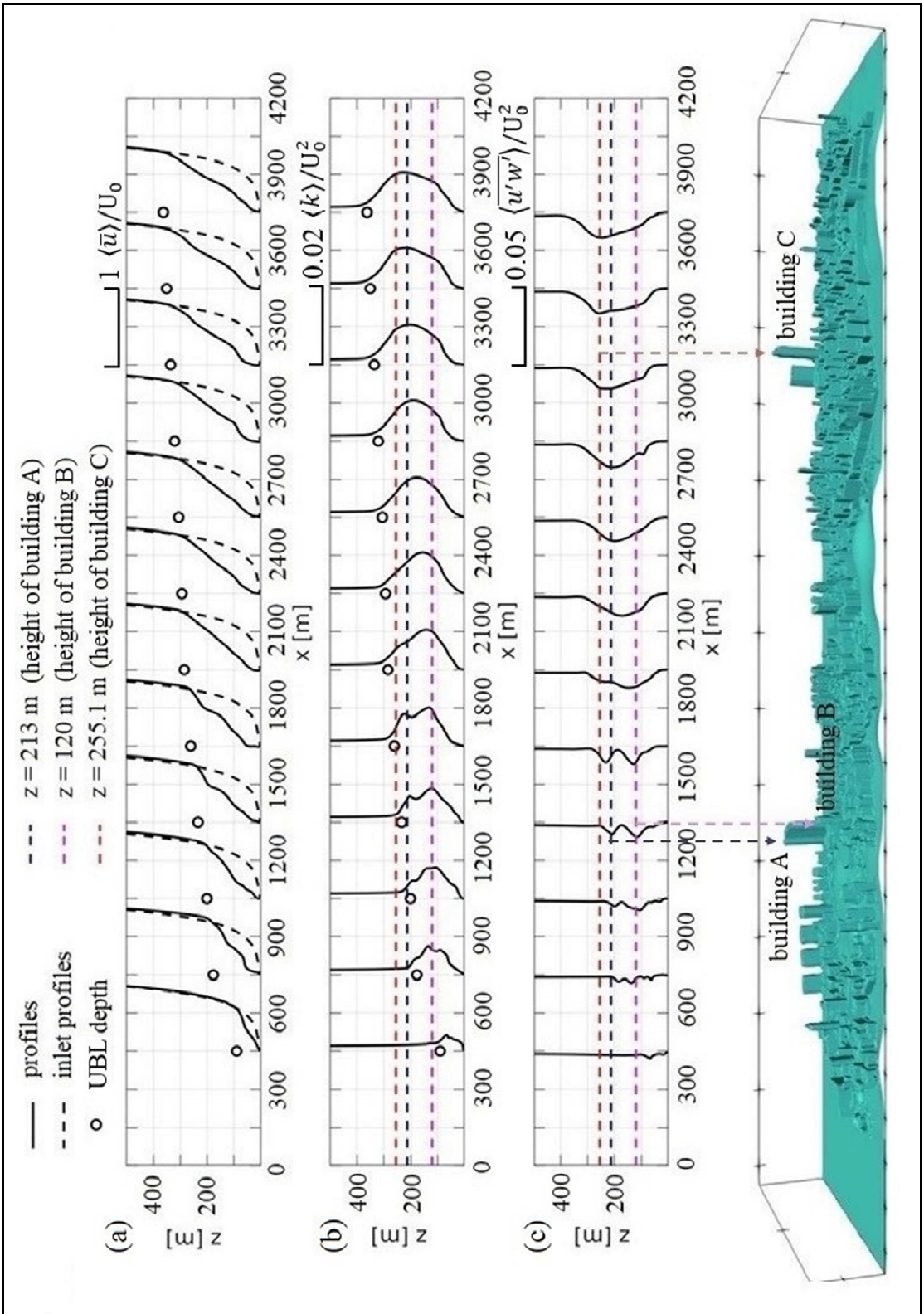

Figure 10: Vertical profiles of horizontal and time averaged properties (a) $\langle \bar{u} \rangle$, (b) $\langle \bar{k} \rangle$ and (c) $\langle \overline{u'w'} \rangle$.

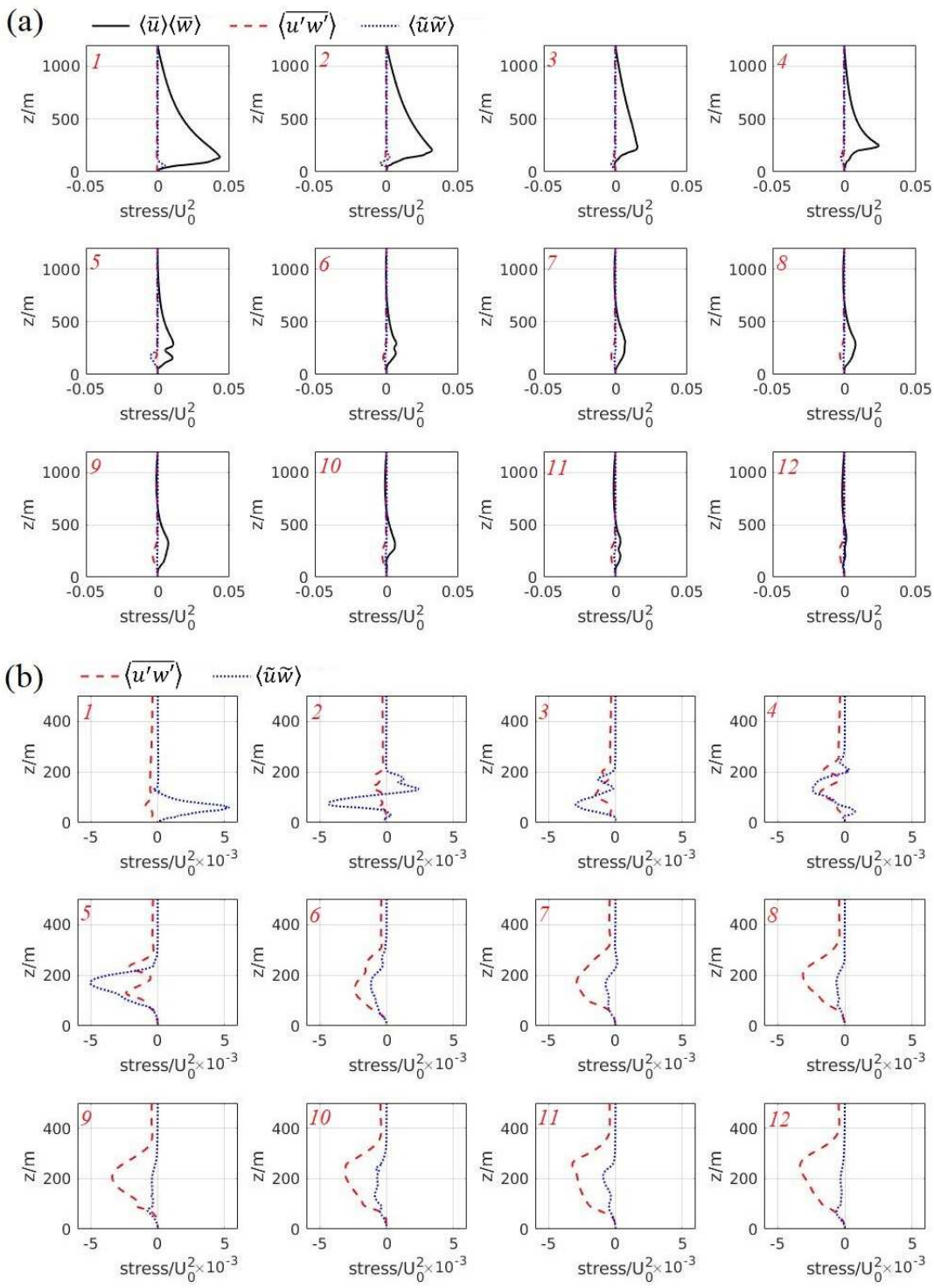

Figure 11: (a) Horizontal and time averaged mean $\langle\bar{u}\rangle\langle\bar{w}\rangle$, turbulent $\langle\overline{u'w'}\rangle$ and dispersive $\langle\tilde{u}\tilde{w}\rangle$ stresses in different zones (labeled by the red number according to those in Fig. 9. (b) Detailed patterns of turbulent $\langle\overline{u'w'}\rangle$ and dispersive $\langle\tilde{u}\tilde{w}\rangle$ stresses plotted in zoomed scale.

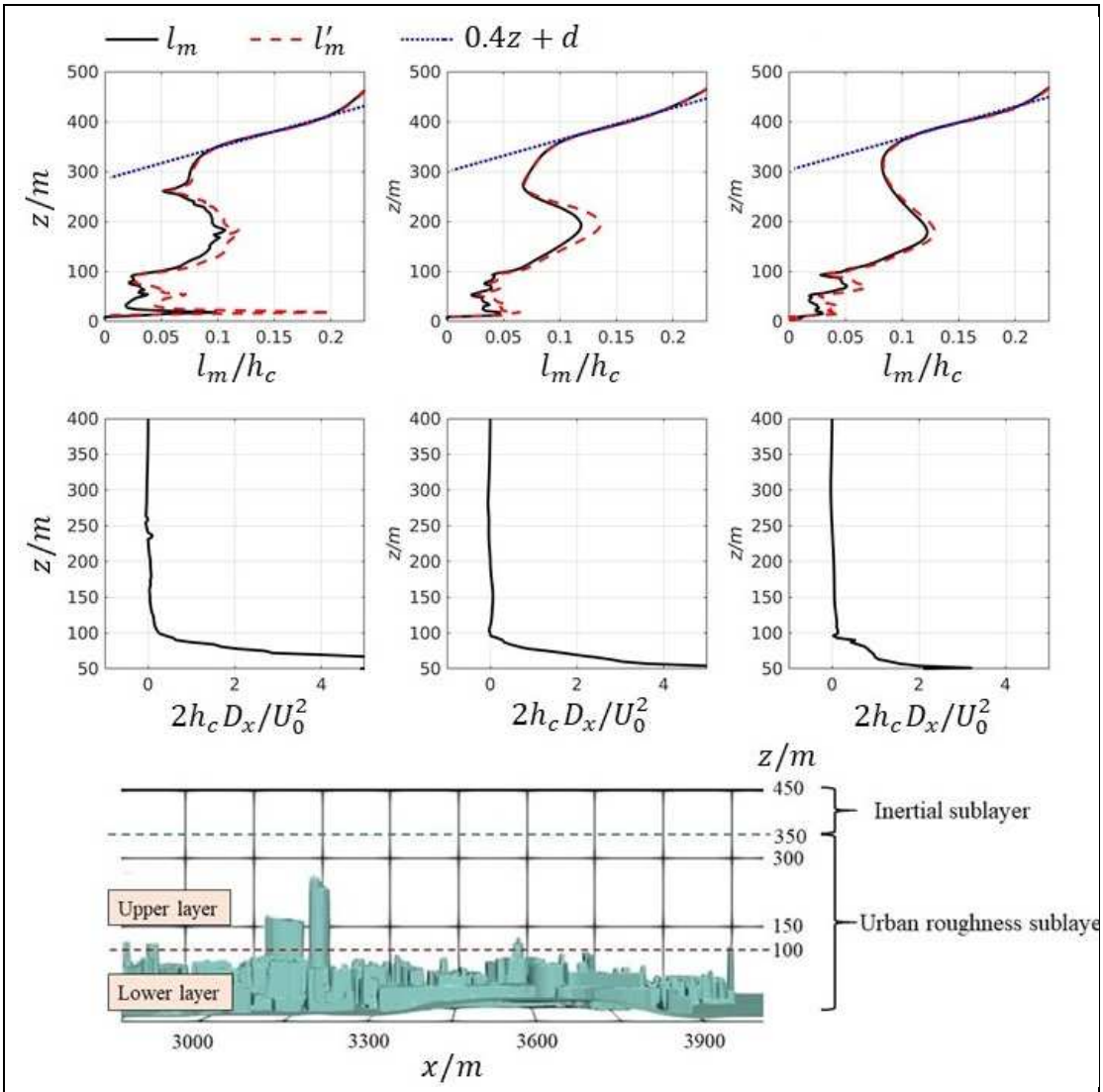

Figure 12: (a) Mixing Length l_m (without dispersive stress), l'_m (with dispersive stress) and (b) effective drag D_x in different zones (labeled by the red number according to those in Fig. 9).